BJR, 2024, **97**, 1557–1567
https://doi.org/10.1093/bjr/tqae122
Advance access publication: 19 June 2024
Research Article

Preoperative prediction of renal fibrous capsule invasion in clear cell renal cell carcinoma using CT-based radiomics model

Yaodan Zhang, MM[1,2,3,4], Jinkun Zhao, MD[1,2,3,4], Zhijun Li, MD, PhD[1,2,3,4], Meng Yang, PhD[2,3,4,5,6,7], Zhaoxiang Ye, MD*[,1,2,3,4]

[1]Department of Radiology, Tianjin Medical University Cancer Institute and Hospital, Tianjin, China
[2]National Clinical Research Center for Cancer, Tianjin, China
[3]Tianjin's Clinical Research Center for Cancer, Tianjin, China
[4]Key Laboratory of Cancer Prevention and Therapy, Tianjin, China
[5]Tianjin Cancer Institute, Tianjin, China
[6]Key Laboratory of Molecular Cancer Epidemiology of Tianjin, Tianjin, China
[7]Tianjin Medical University, Tianjin, China

*Corresponding author: Zhaoxiang Ye, MD, Department of Radiology, Tianjin Medical University Cancer Institute and Hospital, Huan-Hu-Xi Road, Ti-Yuan-Bei, Hexi District, Tianjin 300060, PR China (yezhaoxiang@163.com)

Abstract

Objectives: To develop radiomics-based classifiers for preoperative prediction of fibrous capsule invasion in renal cell carcinoma (RCC) patients by CT images.

Methods: In this study, clear cell RCC (ccRCC) patients who underwent both preoperative abdominal contrast-enhanced CT and nephrectomy surgery at our hospital were analysed. By transfer learning, we used base model obtained from Kidney Tumour Segmentation challenge dataset to semi-automatically segment kidney and tumours from corticomedullary phase (CMP) CT images. Dice similarity coefficient (DSC) was measured to evaluate the performance of segmentation models. Ten machine learning classifiers were compared in our study. Performance of the models was assessed by their accuracy, precision, recall, and area under the receiver operating characteristic curve (AUC). The reporting and methodological quality of our study was assessed by the CLEAR checklist and METRICS score.

Results: This retrospective study enrolled 163 ccRCC patients. The semiautomatic segmentation model using CMP CT images obtained DSCs of 0.98 in the training cohort and 0.96 in the test cohort for kidney segmentation, and DSCs of 0.94 and 0.86 for tumour segmentation in the training and test set, respectively. For preoperative prediction of renal capsule invasion, the AdaBoost had the best performance in batch 1, with accuracy, precision, recall, and F_1-score equal to 0.8571, 0.8333, 0.9091, and 0.8696, respectively; and the same classifier was also the most suitable for this classification in batch 2. The AUCs of AdaBoost for batch 1 and batch 2 were 0.83 (95% CI: 0.68-0.98) and 0.74 (95% CI: 0.51-0.97), respectively. Nine common significant features for classification were found from 2 independent batch datasets, including morphological and texture features.

Conclusions: The CT-based radiomics classifiers performed well for the preoperative prediction of fibrous capsule invasion in ccRCC.

Advances in knowledge: Noninvasive prediction of renal fibrous capsule invasion in RCC is rather difficult by abdominal CT images before surgery. A machine learning classifier integrated with radiomics features shows a promising potential to assist surgical treatment options for RCC patients.

Keywords: clear cell renal cell carcinoma; renal fibrous capsule invasion; radiomics; CT.

Introduction

Renal cell carcinoma (RCC) is a common kidney tumour in urology, of which clear cell RCC (ccRCC) is the predominant subtype and accounts for most cancer-related deaths.[1] The renal fibrous capsule is a tough layer covering the outer surface of the kidney and is surrounded by a perinephric fat layer. According to the tumour-node-metastasis system for RCC staging, renal fibrous capsule invasion is the main risk factor for high-grade ccRCC.[2,3] Minimally invasive techniques, such as partial nephrectomy and percutaneous radiofrequency ablation, are feasible procedures for low-grade ccRCC, while radical operation is a more acceptable treatment for high-grade ccRCC.[4,5] Therefore, preoperative prediction of renal fibrous capsule invasion in ccRCC may be valuable for the clinical treatment options. Renal mass biopsy offers a choice for presurgical diagnosis of renal fibrous capsule invasion. However, the nondiagnostic rate and false-negative error of renal mass biopsy frequently occur. Importantly, as an invasive method, renal mass biopsy may be considered unsafe in certain patients. Therefore, how to accurately evaluate the integrity of renal fibrous capsule in patients with ccRCC based on noninvasive and effective examinations before surgery is an urgent problem for clinicians and radiologists.

Multiphasic contrast-enhanced CT (CECT) scan plays a key role in preoperative RCC assessment. However, the information identified by the naked eye is limited. Many disease characteristics, including the tumour invasion, are

Received: 10 May 2023; **Revised:** 1 May 2024; **Accepted:** 17 June 2024

difficult to distinguish by human vision alone. Radiomics, the high-throughput mining of quantitative image features from medical imaging to improve the accuracy of diagnosis and prediction, is gaining importance in cancer research.[6,7] A growing number of researches have shown that radiomics-derived data can be applied in the preoperative prediction and evaluation of the tumour pathological characteristics.[8,9]

Previous applications of radiomics in RCC mainly included differential diagnosis, subtype classification, and the Fuhrman grade.[10-13] To date, studies of radiomics for the prediction of renal fibrous capsule invasion in RCC are rare. A recent study showed that some radiomic features are related to renal capsule invasion of RCC, but the radiomics models used 2D images instead of 3D CT scan.[14] Moreover, given the limited number of the cases from a single centre, further evaluation and validation for models is necessary based on the larger sample size, independent centres, and different scanners.

In this study, we aimed to develop and validate radiomic models based on abdominal corticomedullary phase (CMP) CT images for preoperative prediction of fibrous capsule invasion in ccRCC patients. Considering that kidney tumours have a deformable shape and poor contrast with respect to the surrounding tissues especially in high-grade RCC, which makes manual segmentation time-consuming and suffers from inter- or intraoperator variations, here we used base model obtained from public Kidney Tumour Segmentation (KiTS) challenge dataset to semi-automatically segment kidney tissues and kidney tumours from abdominal CMP images by transfer learning.[15,16] Currently, most common machine learning classifiers were contained in our study. Based on the radiomics-based model and the significant features, we tried to better evaluate and predict renal fibrous capsule invasion in RCC before surgery.

Materials and methods

Adherence to checklists

This study adhered to the CLEAR checklist[17] and METRICS score[18] for the reporting of our research. The completed CLEAR checklist and METRICS score have been listed in Tables S1 and S2, respectively. The raw data and analysis code that support the findings of this current study are available from the corresponding author on reasonable requests.

Subjects and study design

This study was approved by the Ethics Committee of our hospital. The informed consent requirement was waived. The retrospective study included patients who had undergone radical nephrectomy at our hospital and pathologically confirmed RCC from July 2011 to August 2021. The criteria of patient enrolment were outlined in Figure 1. The inclusion criteria included (1) the patient was histologically confirmed with RCC by surgery; (2) complete abdominal CECT scans were acquired within 2 weeks before the operation; (3) the image quality was satisfactory for analysis: no respiratory and peristaltic artefacts were observed in the images; and (4) whole lesions were clear boundaries on CT images. The exclusion criteria were as follows: (1) other pathological subtypes except for ccRCC; (2) incomplete clinical information; (3) patients received preoperative treatment; (4) histories of any other malignant disease; (5) patients had more than 1 renal lesion. According to their admission time, the patients were divided into 2 batches, respectively from July 2011 to July 2019 as the training group ($n = 103$) and August 2019 to August 2021 as the validation group ($n = 60$). The 2016 WHO/ISUP grading system was used for pathologic staging. Here, we defined ccRCC with histologically confirmed capsule invasion in the following conditions: perinephric fat (+), renal sinus fat (+), or perirenal fibrous layer (+). All data used in this study have not been published or used in any other previous publications. The demographic information for all patients is provided in Table 1.

Imaging acquisition

All included patients underwent an abdominal or abdominal-pelvic CECT scan before surgery. Multiphase-enhanced CT images were obtained using 6 different scanners, including SOMATOM Definition Drive (SIEMENS Medical Solutions, Forchheim, Germany), SOMATOM Definition AS+ (SIEMENS Medical Solutions, Forchheim, Germany), Discovery CT750 HD (GE Medical Systems, Milwaukee, WI, United States), Revolution EVO (GE Medical Systems, Milwaukee, WI, United States), Optima CT680 Expert (GE Medical Systems, Milwaukee, WI, United States), and IQon Spectral CT (Philips Healthcare, Best, Netherlands). The imaging parameters were as follows: tube voltage, 120 kVp; auto tube current; reconstruction section thickness, 1.0-1.5 mm; field of view, 350 mm × 350 mm; matrix, 512 × 512. Images were obtained from the top of the diaphragm to the level of the iliac wing or pubis. The volume of contrast medium was 1.2 mL/kg with an upper limit of 150 mL, a concentration of 300 mg/mL iodine through antecubital vein at the rate of 2.5 mL/s via a high-pressure syringe. Unenhanced CT scan was performed first, and then CMP and nephrographic phase (NP) CT scans were acquired at 28-30 s and 60-70 s delay after contrast medium injection, respectively (Figure 2).

Semiautomatic tumour segmentation

The overall pipeline for the study was summarized in Figure 3. Machine learning models for kidney and tumour segmentation were initially trained on the public KiTS challenge dataset to obtain base models (https://kits19.grand-challenge.org/data/). By using transfer learning,[16] the base models were subsequently adapted to the clinical patients' CMP CT images to get coarse 3D voxel-wise kidney and tumour segmentations. For modelling, 2.5D long-range UNet and short-range ResNet skip connections (ResUNet) were employed for kidney segmentation and a DenseUNet for tumour segmentation (https://github.com/nitsaick/kits19-challenge). The volume of interest of kidney and tumours was checked and adjusted using 3D Slicer software (version 4.8.1) by a radiologist with 7 years of experience. To assess the performance of segmentation models, the spatial overlap was measured using dice similarity coefficient (DSC).

Feature extraction, selection, and classification

Feature extraction was performed using PyRadiomics software (version 2.2.0). Before feature extraction, CT images were resampled into $1.0 \times 1.0 \times 1.0$ mm^3 resolution using linear interpolation. To standardize the intensity range across scanners, Z-score normalization was utilized. The CT images were discretized by fixed bin width and the bin width of the images was 25. Radiomic features were extracted from the

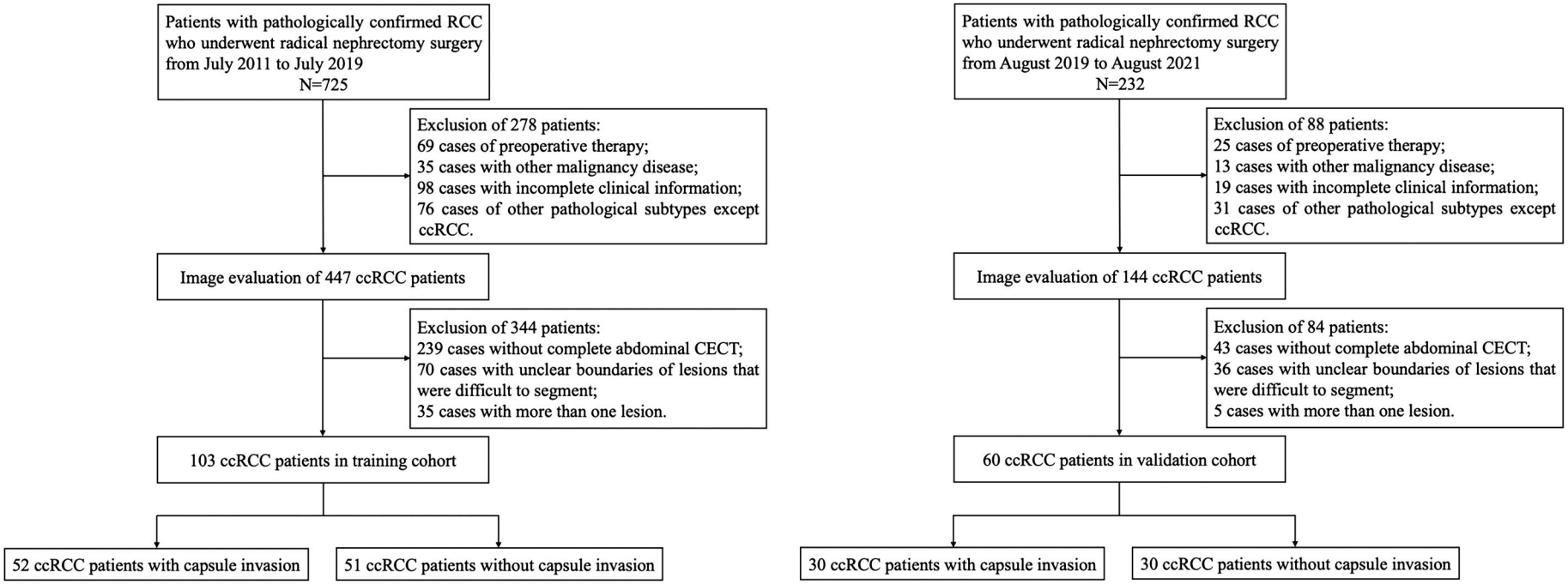

Figure 1. Criteria of patient enrolment in the study. Abbreviations: ccRCC = clear cell renal cell carcinoma; CECT = contrast-enhanced CT.

Table 1. Demographic information of the recruited patients.

Batch	Subset	Number	Age (mean±SD)	Gender
Batch 1	Capsule invasion group	52	59.56 ± 9.05	38 males
	Noncapsule invasion group	51	55.80 ± 10.57	30 males
Batch 2	Capsule invasion group	30	56.67 ± 11.41	21 males
	Noncapsule invasion group	30	57.30 ± 8.58	17 males

original images of tumours. Features with more than 5% incomplete values (ie, unexpected zeros and NA) were regarded as unstable and removed. Remainder of incompleteness were interpolated by their median feature values, outliers, and extreme values were winsorized by nearest interquartile range, respectively. Then, features were scaled into 0-1 by z-score transformation to ensure the comparability of the dynamic range of radiomic features before selection. All other parameters were maintained at their default configurations. The least absolute shrinkage and selection operator algorithm was used to

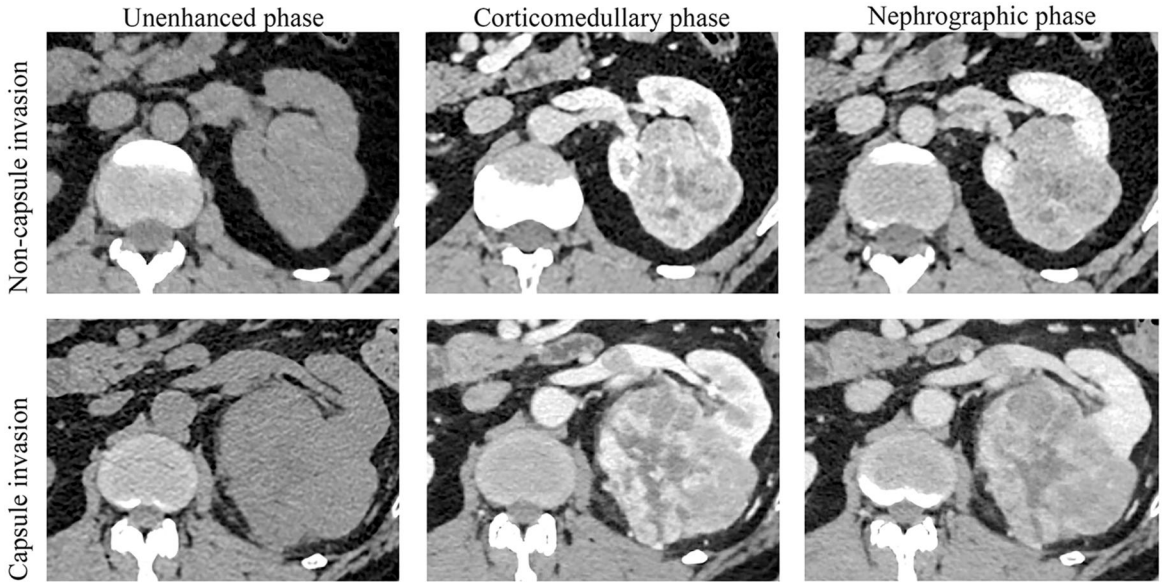

Figure 2. Unenhanced, corticomedullary, and nephrographic phases of ccRCC in 2 groups (noncapsule invasion vs capsule invasion). The tumour invasion is difficult to distinguish by naked eye. Abbreviation: ccRCC = clear cell renal cell carcinoma.

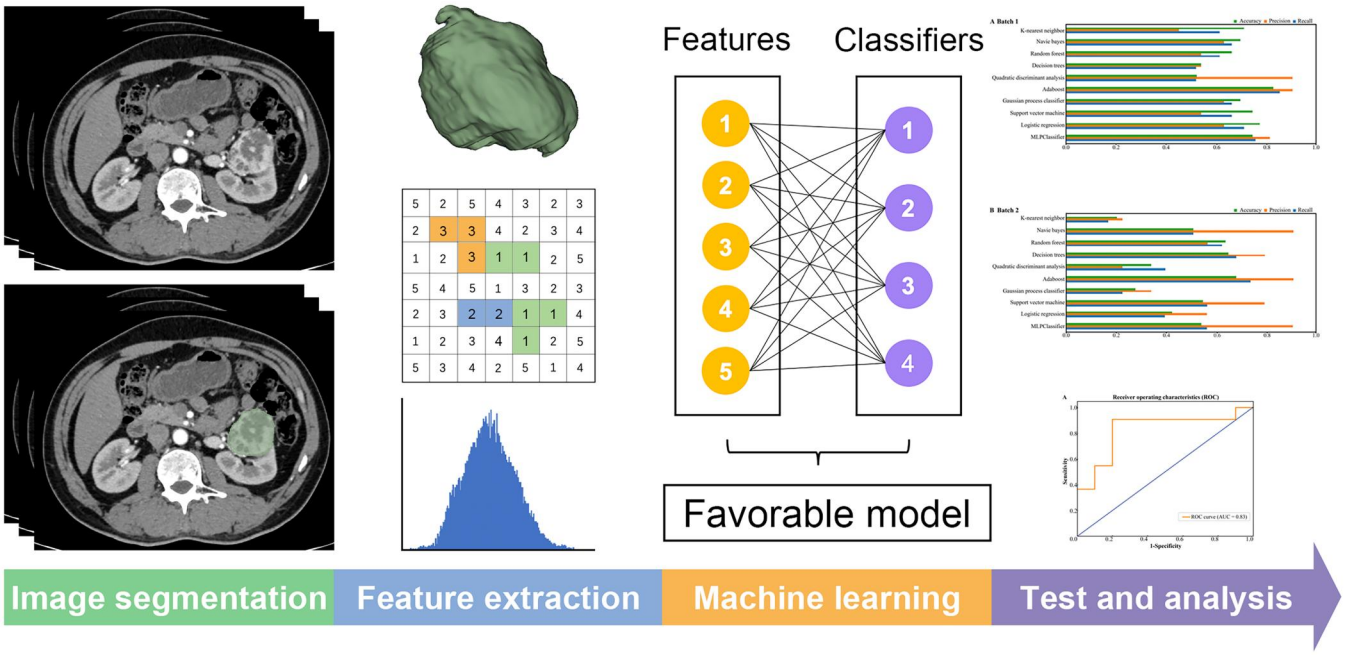

Figure 3. Overall pipeline of the study design.

select a subset of the most related features for machine learning modelling.[19] Random train-test split was used to find the best classification model and optimal hyperparameters on the training set. Feature selection and classifications were performed using an internally developed Python framework in the open-source Python library Scikit-Learn.[20] Common machine learning classifiers were tested on the subset features, including MLPClassifier, logistic regression, support vector machine, Gaussian process classifier, adaptive boosting (AdaBoost), naive Bayes, etc, on batch 1 and batch 2 separately. The parameter configurations of the classifiers are shown in Table S3.

A total of 103 radiomics features were collected and grouped according to first-order, texture, shape 2D and 3D. These categories included shape and morphological features (14 shape features), first-order statistics (19 FOS features), grey-level co-occurrence matrix (24 GLCM features), grey-level dependence matrix (14 GLDM features), grey-level run length matrix (16 GLRLM features), and grey-level scale zone matrix (16 GLSZM features). The features used in classification are provided in Table S4.

Statistical analysis

The difference in clinical characteristics between groups was analysed using Statistical Product and Service Solutions (SPSS 26.0; IBM Corp, Armonk, NY, United States) by hypothesis tests, including Student *t*, Mann-Whitney, and chi-square test. A 2-sided *P* value of <.05 was regarded as statistically significant. DSC was measured to evaluate the performance of segmentation models, which was calculated using the following equation:

$$\mathrm{DSC} = \frac{2 \cdot |\mathrm{SS} \cap \mathrm{PS}|}{|\mathrm{SS}| \cup |\mathrm{PS}|} \quad (1)$$

where SS stands for standard segmentation and PS stands for predicted segmentation. The performance of machine learning classifiers was evaluated by accuracy, precision, and recall. The formulas are as follows:

$$\mathrm{Accuracy} = \frac{(\mathrm{TP}+\mathrm{TN})}{(\mathrm{TP}+\mathrm{FP}+\mathrm{TN}+\mathrm{FN})} \quad (2)$$

$$\mathrm{Precision} = \frac{\mathrm{TP}}{(\mathrm{TP}+\mathrm{FP})} \quad (3)$$

$$\mathrm{Recall} = \frac{\mathrm{TP}}{(\mathrm{TP}+\mathrm{FN})} \quad (4)$$

in which TP and FP represent true positive and false positive, respectively, and TN and FN represent true negative and false negative, respectively. Additionally, receiver operation characteristic (ROC) curve analyses, the area under the ROC curve (AUC), and 95% CIs were also used to quantify the discrimination ability of the classifiers. Furthermore, in order to improve the interpretability for the optimal classifier, we performed the SHapley Additive exPlanations (SHAP).[21]

Results

Reporting and methodological quality assessment

In this study, we applied the CLEAR checklist and METRICS score to guide our research. By using the CLEAR checklist and METRICS score to evaluate the reporting and methodological quality, 51 items are reported in our study, accounting for about 87.9% of the CLEAR checklist; the total METRICS score is 82.7% and the score category is "excellent."

Patient characteristics

The clinical characteristics of all patients are shown in Table 2. Age, sex, and tumour location were not significantly different between the capsule invasion and noncapsule invasion groups. In batch 1, the maximum tumour diameter ranged from 2 to 15 cm in the capsule invasion group, and the lesions were smaller in the noncapsule invasion group (6.90 cm vs 5.04 cm; $P < .001$); however, the maximum tumour diameter was not significantly different in batch 2. The patients with capsule invasion were more poorly differentiated and had higher stages in batch 1 ($P < .001$) and batch 2 ($P = .001$).

Tumour segmentation

A total of 462 cases were enrolled to train the segmentation models, including 299 patients from the public KiTS19 cohort and 163 clinical patients. The patients were separated into a training set ($n = 393$) and a test set ($n = 69$). For kidney

Table 2. Clinical characteristics for 163 patients with ccRCC.

Characteristics	Batch 1 number ($n = 103$)			Batch 2 number ($n = 60$)		
	Capsule invasion group	Noncapsule invasion group	*P* value	Capsule invasion group	Noncapsule invasion group	*P* value
Mean age (range)	60 [36-75]	56 [30-72]	.051	57 [32-74]	57 [37-73]	.809
Sex						
Male	38(73.1%)	30(58.8%)	.127	21(70.0%)	17(56.7%)	.284
Female	14(26.9%)	21(41.2%)		9(30.0%)	13(43.3%)	
Tumour location						
Left	25(48.1%)	24(47.1%)	.918	19(63.3%)	16(53.3%)	.432
Right	27(51.9%)	27(52.9%)		11(36.7%)	14(46.7%)	
Maximum tumour diameter	6.90 [2-15]	5.04 [1.3-18]	<.001	5.78 [5-12]	4.99 [1.8-10.5]	.223
WHO/ISUP grading system						
Grade 1	0 (0.0%)	5 (9.8%)	<.001	0 (0.0%)	1 (3.3%)	.001
Grade 2	8 (15.4%)	32 (62.7%)		10 (33.3%)	23 (76.7%)	
Grade 3	37 (71.2%)	13 (25.5%)		18 (60.0%)	6 (20%)	
Grade 4	7 (13.4%)	1 (2.0%)		2 (6.7%)	0 (0.0%)	

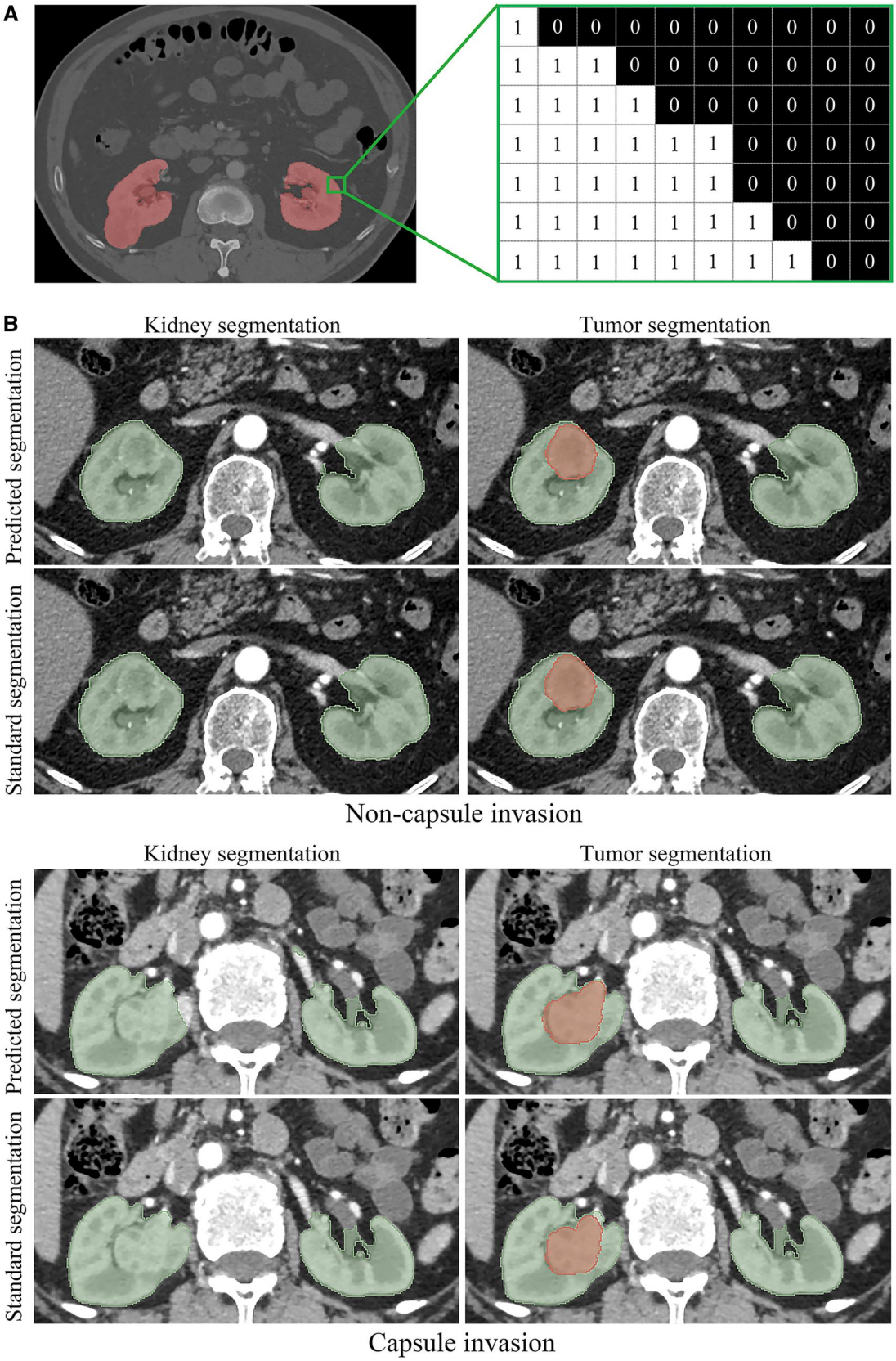

Figure 4. The illustration of segmentation model (A), and examples of the kidney and tumour segmentation results (B).

segmentation, DSC values obtained by CMP CT images were achieved at 0.98 and 0.96 for the training set and test set, respectively; and on tumour segmentation, dice of 0.94 and 0.86 were, respectively, for the training and test set. The example of the kidney and tumour segmentation can be seen in Figure 4.

Performance of radiomics-based classifiers

In batch 1, the radiomics-based classifiers were finally built with 20 features. As shown in Figure 5, we found that the best performance was registered by the AdaBoost among the test classifiers, with accuracy, precision, recall, and F_1-score equal to 0.8571, 0.8333, 0.9091, and 0.8696, respectively. As validation, AdaBoost classifier was also the most suitable classifier for this classification in batch 2, and that is accuracy = 0.7222, precision = 0.6667, recall = 0.8889, and F_1-score = 0.7619. The detailed results are summarized in Table 3. The AUCs of AdaBoost for batch 1 and batch 2 were 0.83 (95% CI: 0.68-0.98) and 0.74 (95% CI: 0.51-0.97), respectively (Figure 6A and B). What is more, we

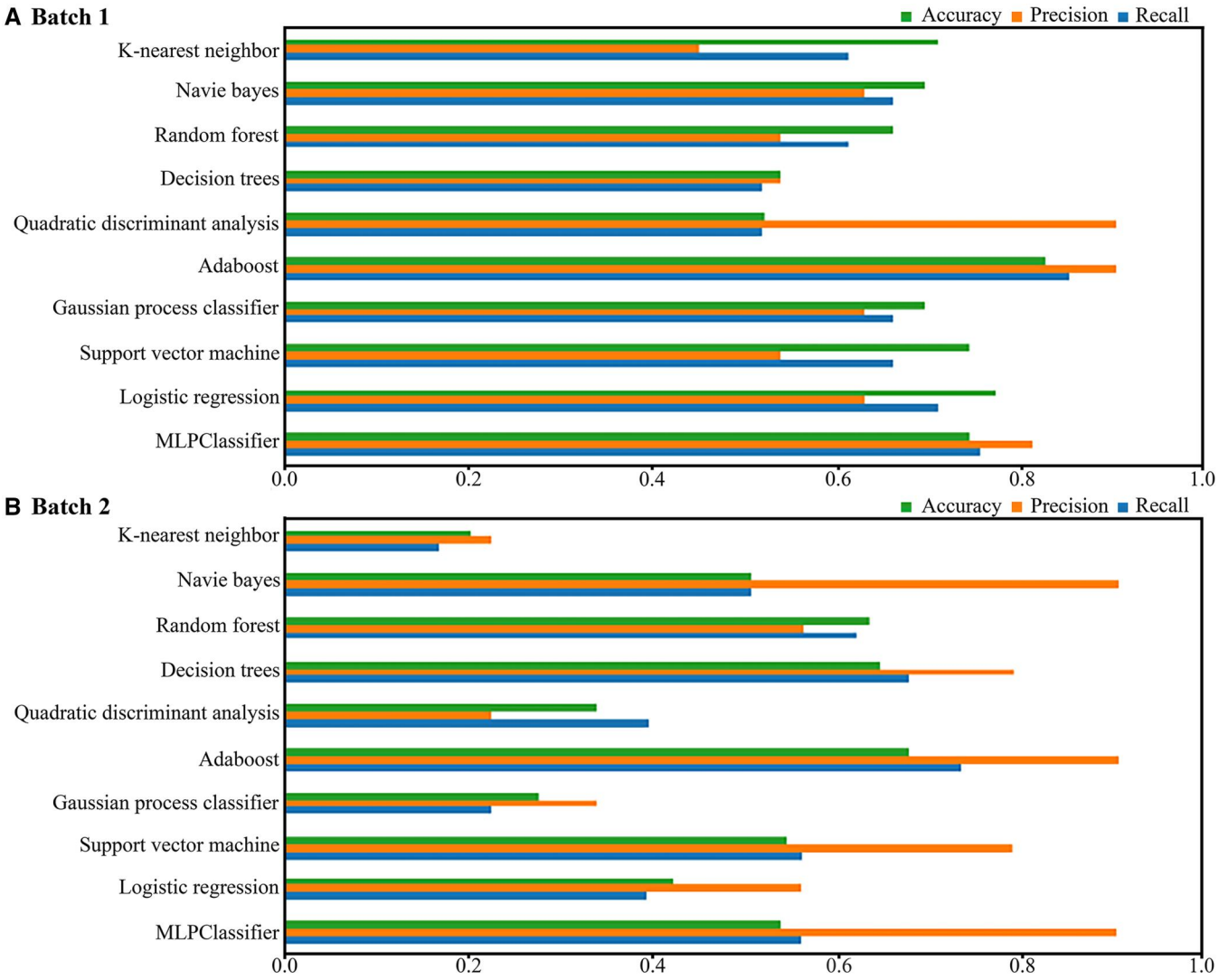

Figure 5. Performance of different classifiers for preoperative prediction of renal fibrous capsule invasion in ccRCC for (A) batch 1 and (B) batch 2. The AdaBoost classifier showed good discrimination ability in 2 batch datasets. Abbreviation: ccRCC = clear cell renal cell carcinoma.

Table 3. Performance of the common classifiers.

Classifiers	Batch 1				Batch 2			
	Accuracy	Precision	Recall	F_1 score	Accuracy	Precision	Recall	F_1 score
MLP Classifier	0.7619	0.8182	0.7500	0.7826	0.5556	0.5333	0. 8889	0.6666
Logistic regression (LR)	0.7143	0.6364	0.7778	0.7000	0.3889	0.5556	0.4167	0.4762
Support vector machine (SVM)	0.6667	0.5454	0.7500	0.6315	0.5556	0.7778	0.5384	0.6363
Gaussian process classifier	0.6667	0.6364	0.7000	0.6667	0.2222	0.3333	0.2727	0.3000
AdaBoost	0.8571	0.8333	0.9091	0.8696	0.7222	0.6667	0.8889	0.7619
Navie Bayes	0.6667	0.6364	0.7000	0.6667	0.5000	0.5000	0.8889	0.6400
Quadratic discriminant analysis (QDA)	0.5238	0.5263	0.9091	0.6666	0.3889	0.2222	0.3333	0.2666
Decision trees	0.5238	0.5455	0.5455	0.5455	0.6667	0.7778	0.6364	0.7000
Random forest	0.6190	0.5455	0.6667	0.6000	0.6111	0.5556	0.6250	0.5883
K-nearest neighbour	0.6190	0.4545	0.7143	0.5555	0.1667	0.2222	0.2000	0.2105

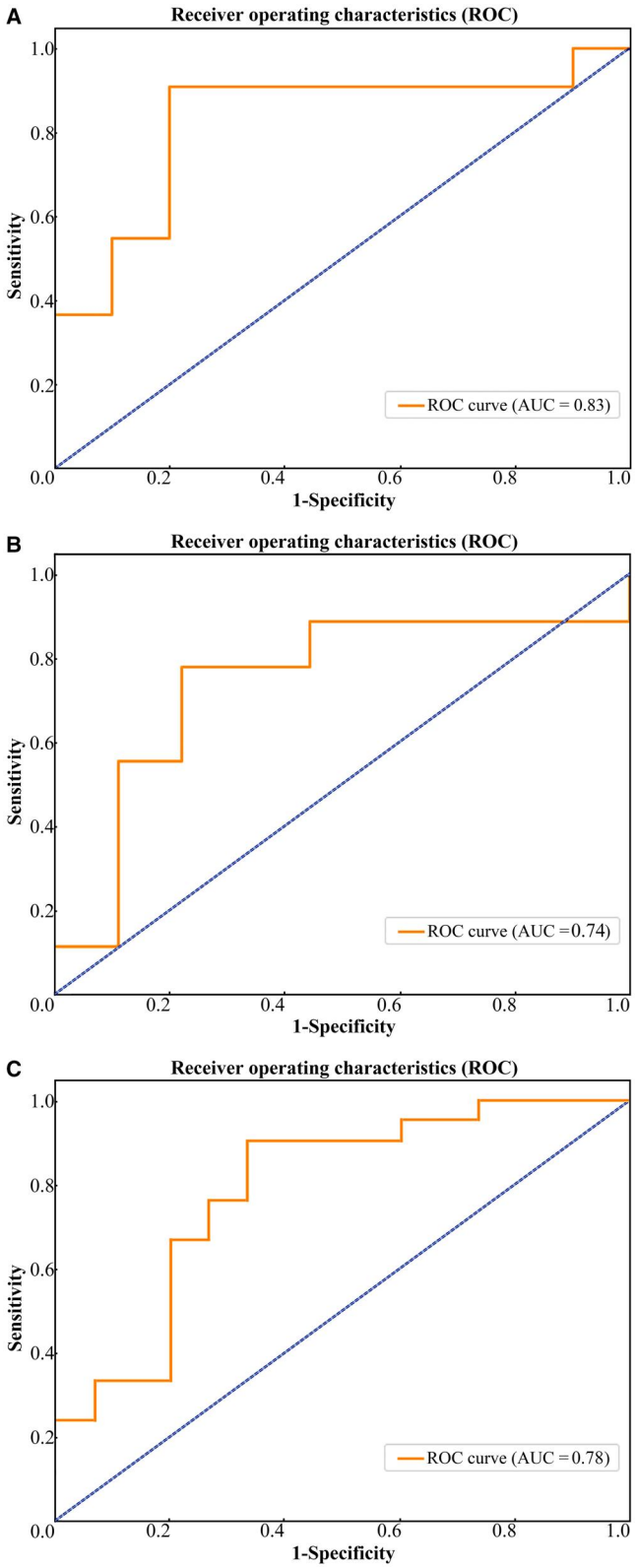

Figure 6. The ROC curves of AdaBoost for (A) batch 1, (B) batch 2 and (C) the combined evaluation of batched 1 and 2. Abbreviations: ccRCC = clear cell renal cell carcinoma; ROC = receiver operating characteristic.

combined batch 1 and batch 2 to evaluate the AdaBoost classifier, with an AUC of 0.78 (95% CI: 0.62-0.93; Figure 6C). The classification metrics of AdaBoost in terms of the data partitions were provided in Table 4. Through the analyses of 2 independent batch datasets, we found several common significant features for building classification models, which are divided into morphological and texture parts. The common morphological features include flatness, sphericity, and maximum diameter. For texture parts, the common features of batches contain firstorder_skewness, firstorder_minimum, firstorder_interquartile range, grey level co-occurrence matrix (GLCM)_ cluster shade, grey level size zone matrix (GLSZM)_ small area emphasis (SAE), and grey level dependence matrix (GLDM)_ large dependence high grey level emphasis (LDHGLE).

Interpretability of the optimal classifier

The SHAP value was used to obtain the importance of each feature for the AdaBoost classifier. Figure 7 is the SHAP summary plot and presents the most significant features in descending order according to the mean absolute SHAP value. The average of GLCM_ Inverse Variance had the most important value for all prediction features, followed quite closely by GLSZM_ size-zone non-uniformity (SZN), shape_ flatness, GLSZM_ grey level non-uniformity normalized, and GLSZM_ SAE.

Discussion

In the current study, we confirmed radiomics-based classifiers could predict fibrous capsule invasion in RCC patients before surgery by using abdominal CMP CT images. What's more, the AdaBoost classifier showed good discrimination ability in 2 batch datasets from different admission time and different scanners.

Currently, the accurate evaluation of fibrous capsule invasion in RCC patients still relies on postoperative pathology, and what CT images can provide before surgery is just confined to morphological characteristics, including large size, edge blur, and exophytic appearance.[22,23] Nevertheless, because of the tumour heterogeneity of RCC, it is difficult to discriminate fibrous capsule invasion by the naked eyes. In our study, the radiomics-based AdaBoost classifier showed good predictive power, which combined more detailed information on tumour 2D and 3D shape features, first-order statistics, second-order joint probability function, and others. The common shape features of batches indicate that the tumour edge and size may have more effect on diagnosis for fibrous capsule invasion of the lesion, even high-grade RCC.[24,25] However, the maximum tumour diameter had no statistical significance in batch 2 when we analysed the difference in clinical characteristics between the 2 groups. The probable explanation was the small sample size. And the significant texture features, like GLSZM_ SAE and GLDM_ LDHGLE, which have a greater value, respectively, indicative of more small size that share the same grey-level intensity and is more homogeneous with higher grey-level values, suggest the tumour with fibrous capsule invasion may have larger obviously enhanced area but be more inhomogeneous for the overall enhancement. This conclusion is also consistent with the enhancement of high-grade RCC, meaning that renal capsule invasion is a significant risk factor for the grading of RCC.[26,27] In addition, by calculating the SHAP value to evaluate the importance of features in the optimal classifier, we found that local texture features of the lesion would have more influence on the radiomics-based classification models.

Table 4. Classification performance of AdaBoost on different data partitions.

Performance metrics	Data partitions		
	Training set (batch 1)	Validation set (batch 2)	Whole data (batches 1 and 2)
Accuracy	0.857	0.722	0.818
Sensitivity	0.909	0.889	0.892
Specificity	0.800	0.556	0.750
Precision	0.833	0.667	0.789
Negative predictive value	0.889	0.833	0.857
F_1	0.870	0.762	0.833
AUROC	0.827 (0.680 - 0.980)	0.741 (0.511-0.969)	0.779 (0.622 -0.930)

Abbreviation: AUROC = area under the receiver operating characteristic curve.

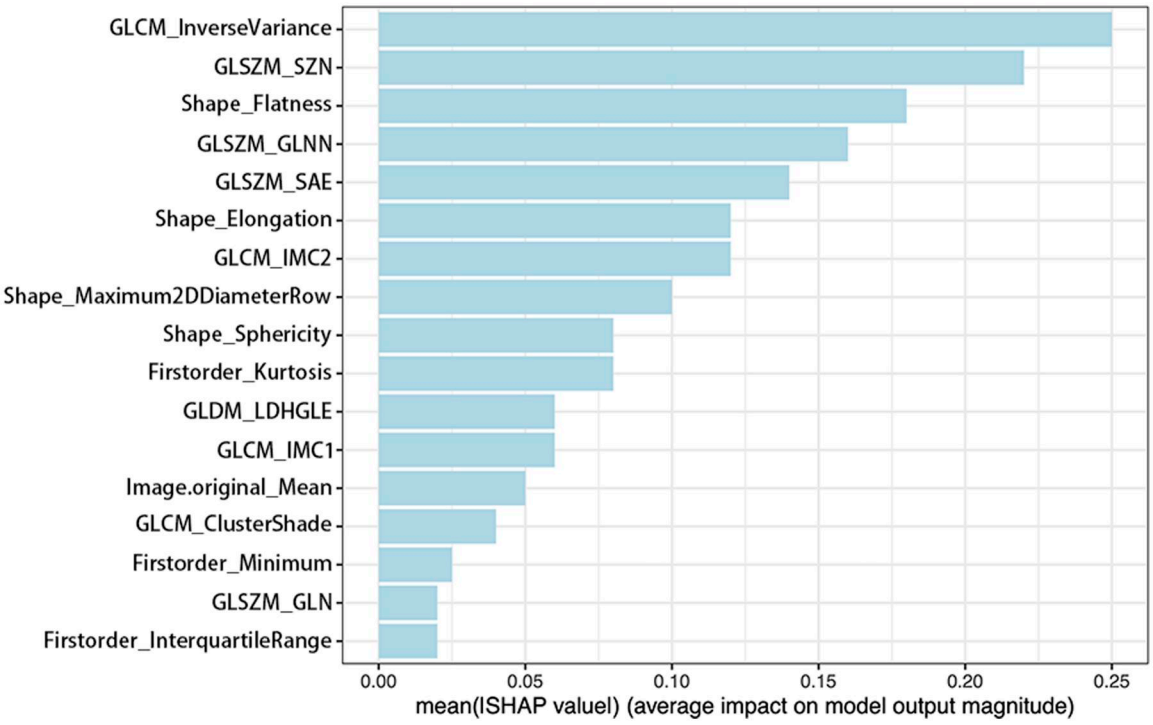

Figure 7. The SHAP values and weights of features importance. Abbreviations: GLCM = grey-level co-occurrence matrix; GLDM = grey-level dependence matrix; GLN = grey-level non-uniformity; GLNN = grey-level non-uniformity normalized; GLSZM = grey-level scale zone matrix; LDHGLE = large dependence high grey-level emphasis; IMC = informational measure of correlation; SHAP = SHapley Additive exPlanations; SZN = size-zone non-uniformity.

Previous studies of periphery and peritumour situations of RCC are mainly based on ultrasound and MRI.[28-30] Nevertheless, as we know, ultrasound is highly operator-dependent, while MRI is not the routine preoperative test for clinical RCC patients. Recently, some research has noticed the potential of CT signs for estimating fibrous capsule invasion in RCC before procedure, and some also reported the related radiomics-based classification models using CT images.[14,31,32] Because of the limited cases from single centre, further validation for the models and findings was necessary. Our study contained 2 independent batches of ccRCC patients and, respectively, estimated the performance of radiomics-based classifiers for predicting renal fibrous capsule invasion. Additionally, our models applied 3D CT images, which could more comprehensively assess the detailed information of tumour.

To our knowledge, manually 3D delineation of lesions is a challenge for radiologists, which is time-consuming and may introduce intra and interobserver variability. Transfer learning, as the reuse of a pre-trained model, is popular in machine learning for it can train deep neural networks with relatively little data.[33,34] In our study, base model obtained from CMP CT images of public KiTS challenge dataset was used to semi-automatically segment kidney and tumours of our clinical RCC patients, which enabled the segmentation more efficient. The final semiautomatic model showed high segmentation accuracy in the training set with DSCs of 0.98 and 0.94, respectively, for kidney and tumour segmentation, which was validated in the test set with DSCs of 0.96 and 0.86, respectively.

In our study, we evaluated the performance of classifiers applied to predict renal fibrous capsule invasion in ccRCC before surgery by accuracy, precision, recall, and F_1-score, which are the most common evaluation indicators in the classification model of machine learning.[35] During the batch 1 and batch 2 analyses, AdaBoost classifier was both the most

suitable classifier for this classification, and in batch 1, the accuracy, precision, recall, and F_1-score of the classifier were equal to 0.8571, 0.8333, 0.9091, and 0.8696, respectively. Of note, among all indicators of the AdaBoost that were generally the highest compared with other classifiers, the precision and recall values are interrelated and affected each other, which decrease may respectively cause misdiagnosis and overdiagnosis.[36] And in our study, the precision and recall value of the optimized AdaBoost are both relatively satisfactory. Therefore, it is also suggested that the radiomics-based model may have the potential as an alternative to preoperatively evaluate the renal fibrous capsule invasion for ccRCC patients in the future clinical practice. Besides, this study still has some limitations. First, our study only focuses on the images from CT scans, multisequence and enhanced MR should be analysed in further studies. Secondly, serum biomarkers and genomic variants should be concerned in future work. Finally, our classifiers were trained by one-centre samples, larger samples from different institutions would prove the reproducibility of our model.

In conclusion, we developed a radiomics-based model from CT images with favourable accuracy for the preoperative evaluation of renal fibrous capsule invasion in ccRCC. The results show an association between radiomics features in abdominal CMP CT images and renal capsule invasion of RCC. This radiomics model holds the promising potential as a non-invasive approach for the prediction of the risk of renal fibrous capsule invasion in ccRCC before operation and may be valuable for the selection of surgical treatment in clinical decision-making.

Supplementary material

Supplementary material is available at *BJR* online.

Funding

This work was supported by the National Key R&D Program of China (2021YFC2500402), and Tianjin Key Medical Discipline (Specialty) Construction Project (TJYXZDXK-009A). The funders had no role in study design, data analysis, decision to publish, or preparation of manuscript.

Conflicts of interest

The authors declare no competing financial interests or personal relationships that could have appeared to influence the work reported in this paper.

References

1. Bray F, Ferlay J, Soerjomataram I, Siegel RL, Torre LA, Jemal A. Global cancer statistics 2018: GLOBOCAN estimates of incidence and mortality worldwide for 36 cancers in 185 countries. *CA Cancer J Clin*. 2018;68(6):394-424.
2. Ha U-S, Lee KW, Jung J-H, et al. Renal capsular invasion is a prognostic biomarker in localized clear cell renal cell carcinoma. *Sci Rep*. 2018;8(1):202.
3. Amin MB, Edge SB, Greene FL, Byrd DR, Brookland RK, Washington MK, et al. AJCC Cancer Staging Manual. In: *AJCC Cancer Staging Manual*. 8th ed. Cham: Springer International Publishing; 2017.
4. Mir MC, Derweesh I, Porpiglia F, Zargar H, Mottrie A, Autorino R. Partial nephrectomy versus radical nephrectomy for clinical T1b and T2 renal tumors: a systematic review and meta-analysis of comparative studies. *Eur Urol*. 2017;71(4):606-617.
5. Jiang YL, Peng CX, Wang HZ, Qian LJ. Comparison of the long-term follow-up and perioperative outcomes of partial nephrectomy and radical nephrectomy for 4 cm to 7 cm renal cell carcinoma: a systematic review and meta-analysis. *BMC Urol*. 2019;19(1):48.
6. Mayerhoefer ME, Materka A, Langs G, et al. Introduction to radiomics. *J Nucl Med*. 2020;61(4):488-495.
7. van Griethuysen JJM, Fedorov A, Parmar C, et al. Computational radiomics system to decode the radiographic phenotype. *Cancer Res*. 2017;77(21):e104-e107.
8. Gao X, Ma T, Cui J, et al. A radiomics-based model for prediction of lymph node metastasis in gastric cancer. *Eur J Radiol*. 2020;129:109069.
9. Erdim C, Yardimci AH, Bektas CT, et al. Prediction of benign and malignant solid renal masses: machine learning-based CT texture analysis. *Acad Radiol*. 2020;27(10):1422-1429.
10. Cui E-M, Lin F, Li Q, et al. Differentiation of renal angiomyolipoma without visible fat from renal cell carcinoma by machine learning based on whole-tumor computed tomography texture features. *Acta Radiol*. 2019;60(11):1543-1552.
11. Ding J, Xing Z, Jiang Z, et al. CT-based radiomic model predicts high grade of clear cell renal cell carcinoma. *Eur J Radiol*. 2018;103:51-56.
12. Bektas CT, Kocak B, Yardimci AH, et al. Clear cell renal cell carcinoma: machine learning-based quantitative computed tomography texture analysis for prediction of Fuhrman nuclear grade. *Eur Radiol*. 2019;29(3):1153-1163.
13. Bhandari A, Ibrahim M, Sharma C, Liong R, Gustafson S, Prior M. CT-based radiomics for differentiating renal tumours: a systematic review. *Abdom Radiol (NY)*. 2021;46(5):2052-2063.
14. Yang L, Gao L, Arefan D, Tan Y, Dan H, Zhang J. A CT-based radiomics model for predicting renal capsule invasion in renal cell carcinoma. *BMC Med Imaging*. 2022;22(1):15.
15. Heller N, Sathianathen N, Kalapara A, et al. The KiTS19 challenge data: 300 kidney tumor cases with clinical context, ct semantic segmentations, and surgical outcomes, arXiv, preprint: not peer reviewed. https://doi.org/10.48550/arXiv.1904.00445
16. Pan SJ, Yang Q. A survey on transfer learning. *IEEE Trans Knowl Data Eng* 2010;(10):22.
17. Kocak B, Baessler B, Bakas S, et al. CheckList for EvaluAtion of Radiomics research (CLEAR): a step-by-step reporting guideline for authors and reviewers endorsed by ESR and EuSoMII. *Insights Imaging*. 2023;14(1):75.
18. Kocak B, Akinci D'Antonoli T, Mercaldo N, et al. METhodological RadiomICs Score (METRICS): a quality scoring tool for radiomics research endorsed by EuSoMII. *Insights Imaging*. 2024;15(1):8.
19. Jolliffe IT, Trendafilov NT, Uddin M. A modified principal component technique based on the LASSO. *J Comput Graph Stat* 2003;12(3):531-547.
20. Pedregosa F, Varoquaux G, Gramfort A, et al. Scikit-Learn: machine learning in Python. *J Mach Learn Res* 2011;12:2825-2830.
21. Lundberg SM, Lee SI. A unified approach to interpreting model predictions. NIPS'17. 2017; 4768-4777. https://doi.org/10.48550/arXiv.1705.07874
22. Thomas DH, Verghese A, Kynaston HG, Griffiths DF. Analysis of the prognostic implications of different tumour margin types in renal cell carcinoma. *Histopathology*. 2003;43(4):374-380.
23. Delahunt B, Eble JN, Samaratunga H, Thunders M, Yaxley JW, Egevad L. Staging of renal cell carcinoma: current progress and potential advances. *Pathology*. 2021;53(1):120-128.
24. Chen C, Kang Q, Xu B, et al. Differentiation of low- and high-grade clear cell renal cell carcinoma: Tumor size versus CT perfusion parameters. *Clin Imaging*. 2017;46:14-19.

25. Zhang X, Zhang G, Xu L, et al. Prediction of World Health Organization/International Society of Urological Pathology (WHO/ISUP) pathological grading of clear cell renal cell carcinoma by dual-layer spectral CT. *Acad Radiol*. 2022;30(10):2321-2328.
26. Coy H, Young JR, Douek ML, et al. Association of qualitative and quantitative imaging features on multiphasic multidetector CT with tumor grade in clear cell renal cell carcinoma. *Abdom Radiol (NY)*. 2019;44(1):180-189.
27. Coy H, Young JR, Pantuck AJ, et al. Association of tumor grade, enhancement on multiphasic CT and microvessel density in patients with clear cell renal cell carcinoma. *Abdom Radiol (NY)*. 2020;45(10):3184-3192.
28. Oh TH, Lee YH, Seo IY. Diagnostic efficacy of contrast-enhanced ultrasound for small renal masses. *Korean J Urol*. 2014;55(9):587-592.
29. Zhang H, Wu Y, Xue W, et al. Arterial spin labelling MRI for detecting pseudocapsule defects and predicting renal capsule invasion in renal cell carcinoma. *Clin Radiol*. 2017;72(11):936-943.
30. Papalia R, Panebianco V, Mastroianni R, et al. Accuracy of magnetic resonance imaging to identify pseudocapsule invasion in renal tumors. *World J Urol*. 2020;38(2):407-415.
31. Zhang Y, Tian H, Zhang S, Zhang Q, Wu X. Multislice spiral computed tomography signs of invasion of the renal capsule by renal cell carcinoma. *Medicine (Baltimore)*. 2018;97(44):e13075.
32. Fateh SM, Arkawazi LA, Tahir SH, et al. Renal cell carcinoma T staging: diagnostic accuracy of preoperative contrast-enhanced computed tomography. *Mol Clin Oncol*. 2023;18(2):11.
33. Marinelli B, Kang M, Martini M, et al. Combination of active transfer learning and natural language processing to improve liver volumetry using surrogate metrics with deep learning. *Radiol Artif Intell*. 2019;1(1):e180019.
34. Kim HE, Cosa-Linan A, Santhanam N, Jannesari M, Maros ME, Ganslandt T. Transfer learning for medical image classification: a literature review. *BMC Med Imaging*. 2022;22(1):69.
35. Hand DJ, Christen P, Kirielle N. F*: an interpretable transformation of the F-measure. *Mach Learn*. 2021;110(3):451-456.
36. Powers DMW. Evaluation: from precision, recall and F-factor to ROC, informedness, markedness and correlation, arXiv, 2008, preprint: not peer reviewed. https://doi.org/10.48550/arXiv.2010.16061

British Journal of Radiology, 2024, 97, 1557–1567
https://doi.org/10.1093/bjr/tqae122
Research Article